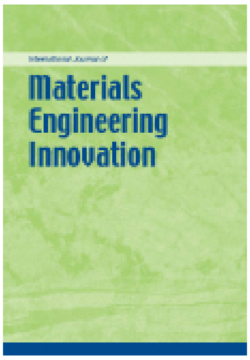

International Journal of Materials Engineering Innovation

ISSN online: 1757-2762 - ISSN print: 1757-2754
https://www.inderscience.com/ijmatei

Anti-tetrachiral auxetic structures fabricated by material extrusion: numerical and experimental investigation on influence of design parameters on mechanical properties under compressive loading

Soham Teraiya, Swapnil Vyavahare, Shailendra Kumar

DOI: 10.1504/IJMATEI.2023.10051278

Article History:

Received:	11 March 2022
Accepted:	16 April 2022
Published online:	25 March 2024

Anti-tetrachiral auxetic structures fabricated by material extrusion: numerical and experimental investigation on influence of design parameters on mechanical properties under compressive loading

Soham Teraiya, Swapnil Vyavahare and Shailendra Kumar*

Department of Mechanical Engineering,
Sardar Vallabhbhai National Institute of Technology,
Surat, Gujarat-395007, India
Email: sohamteraiya@gmail.com
Email: swapnil.vyavahre@gmail.com
Email: skbudhwar@med.svnit.ac.in
Email: skbudhwar@gmail.com
*Corresponding author

Abstract: The present article describes a numerical and experimental investigation on mechanical properties of anti-tetrachiral auxetic structures under compressive loading. The structures of acrylonitrile butadiene styrene material are fabricated by material extrusion technique of additive manufacturing. The influence of design parameters namely node radius and ligament thickness is studied on responses including strength, modulus and specific energy absorption (SEA) of in-plane and out-of-plane oriented structures. Experiments are planned using face-centred central composite design. From the experimental study, it is found that both design parameters significantly influence strength, modulus and SEA of structures. Also, it is observed that the stresses in plateau region of stress-strain curve remain almost constant till the densification phase during compressive loading of in-plane oriented structure, while the strength and modulus are high in out-of-plane oriented structure. Further, regression models for strength, modulus and SEA are developed, and optimisation of design parameters is performed to maximise the responses.

Keywords: mechanical properties; anti-tetrachiral auxetic structure; compressive loading; material extrusion; additive manufacturing; design parameters; strength; modulus.

Reference to this paper should be made as follows: Teraiya, S., Vyavahare, S. and Kumar, S. (2024) 'Anti-tetrachiral auxetic structures fabricated by material extrusion: numerical and experimental investigation on influence of design parameters on mechanical properties under compressive loading', *Int. J. Materials Engineering Innovation*, Vol. 15, No. 1, pp.33–65.

Biographical notes: Soham Teraiya is pursuing his PhD under supervision of Dr. Shailendra Kumar at Sardar Vallabhbhai National Institute of Technology (SVNIT), Surat, India. He completed his MTech in Manufacturing Engineering from the same institute in 2015. His research areas include additive manufacturing, auxetic structures and automatic feature recognition.

Swapnil Vyavahare has completed his PhD under supervision of Dr. Shailendra Kumar at SVNIT, Surat, India. He completed his MTech in CAD/CAM from Veermata Jijabai Technological Institute, Mumbai, India in 2011. His research areas include additive manufacturing, artificial neural network and auxetic structures.

Shailendra Kumar is working as a Professor at the Department of Mechanical Engineering, SVNIT, Surat, India. He has more than 20 years of teaching, research and administrative experience. He completed five research projects funded by various national and international agencies. More than 160 research papers in various international and national journals as well as international and national conferences are at his credit. He is interested in research areas including additive manufacturing, AI applications in sheet metal forming, and modern machining processes.

1 Introduction

Cellular structures are widely used in various applications such as aerospace, automotive, sports, and medical industries due to their higher strength to weight ratio and energy absorption capabilities (Gibson and Ashby, 1997; Ashby, 2006; Paulino et al., 2009; Vesenjak et al., 2009; Zhu et al., 2009; Larcher, 2011; Sousa-Martins and Teixeira-Dias, 2011; Xu et al., 2020). Auxetic structure is a recently developed cellular structure that exhibits superior mechanical properties. Due to its unique structural geometry, auxetic structures have a negative Poisson's ratio (NPR) (Lakes, 1987). Unlike conventional structures, which expand under compressive loading, the auxetic structures contract in a lateral direction under compression loading due to its NPR. They exhibit superior mechanical properties such as good indentation resistance, large shear modulus, high fracture toughness, synclastic shape under bending moment, and unique acoustic properties (Kolken and Zadpoor, 2017; Sarvestani et al., 2018). Auxetic structures are used in a wide range of applications such as automotive crash box, robust shock absorbers, fasteners, air seat cushions, sound absorbers, air filters and mass filters (Alderson et al., 2000; Bezazi and Scarpa, 2007; Grima et al., 2008; Scarpa et al., 2004; Imbalzano et al., 2017; Dalela et al., 2021). There are various types of auxetic structures such as re-entrant, tetra-chiral, anti-tetrachiral, trichiral, anti-trichiral, hexachiral, re-entrant chiral, star shaped, lozenge grid, and double arrowhead structures, etc. (Kolken and Zadpoor, 2017; Alomarah et al., 2020a; Vyavahare and Kumar, 2021; Kumar et al., 2021). Among these structures, the deformation mechanism of chiral structures is unique, as the load is transferred to the ligament via rotating nodes (Prall and Lakes, 1997). The structures with three, four and six ligaments connected to the single node are called trichiral, tetrachiral and hexachiral respectively. If nodes are connected on the opposite side of the structure, it is called chiral structures, while if nodes are connected on the same side of the ligament, it is called anti-chiral structure. Anti-tetrachiral structures exhibit better auxeticity, modulus and energy absorption compared to other auxetic structures (Alderson et al., 2010; Najafi et al., 2021). In these structures, four ligaments are tangentially connected to a single node at 90° in which each adjacent node is connected on the same side of the ligaments. Anti-tetrachiral structures are used in various applications, namely wing box, shape-memory structures, airfoil morphing, biomedical stent, tyres, vibration attenuation, impact detection sensors, and other energy absorbing structures (Abramovitch et al., 2010; Wu et al., 2019, 2021). Design parameters of the structure play a crucial role in improvement of mechanical properties of the part (Vyavahare and Kumar, 2021). Manufacturing of these structures using conventional manufacturing processes such as casting, welding and forming is challenging due to its complex geometry, higher cost and lead time of tooling. It can be easily fabricated with good dimensional accuracy by material extrusion (ME) technique of additive manufacturing (AM) (Singh and Pandey, 2015). ME is extensively used in various applications such as medical, jewellery, aerospace, automotive, dental, art and sports industries (Kumar et al., 2012; Gibson et al., 2015; Fernandes et al., 2016; Meneses et al., 2016; Boparai and Singh, 2019; Kumar and Vinodh, 2019). The feedstock materials such as acrylonitrile butadiene styrene (ABS), polylactic acid (PLA), polyethylene terephthalate glycol (PETG), high impact polystyrene (HIPS) is supplied in the form of wire and molten material is extruded through the nozzle of the machine. The components are produced in a layer-by-layer fashion. ME process provides maximum design flexibility and control over the variation of design parameters of the auxetic structure (Vyavahare and Kumar, 2020). The schematic of ME process is shown in Figure 1.

Figure 1 Schematic of material extrusion (see online version for colours)

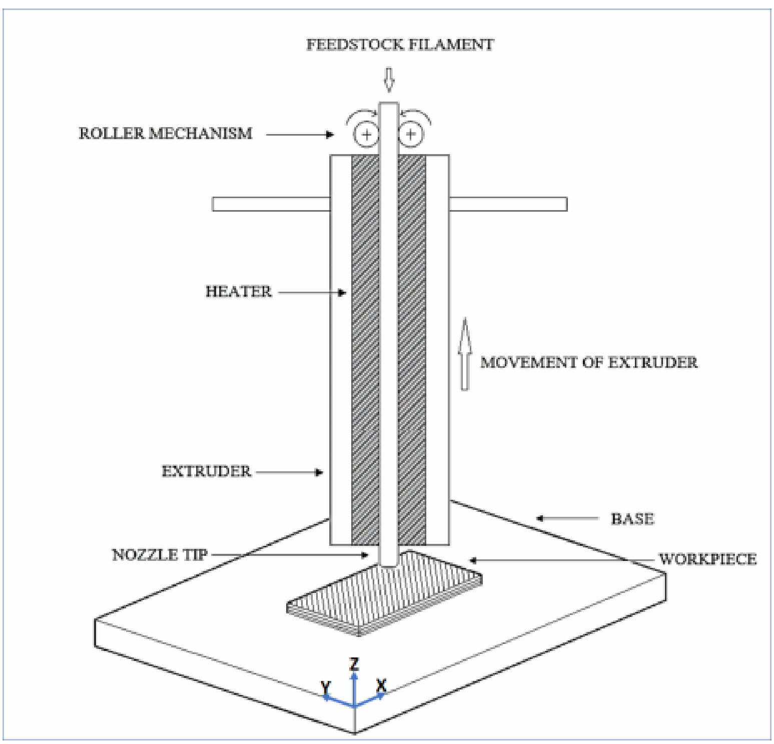

Worldwide researchers investigated the properties of auxetic cellular structures using numerical, experimental and analytical methods. Grima et al. (2008) developed meta tetrachiral structures by changing the constraints of rotational geometry of the structure.

The developed analytical models are useful in controlling the Poisson's ratio, thus tailoring the properties of structure according to a specific application. Lorato et al. (2010) studied the out-of-plane mechanical properties of the trichiral, anti-trichiral, tetrachiral, anti-tetrachiral and hexachiral structures. The analytical and numerical models developed by them were used to determine the Young's modulus and traverse shear stiffness of the structures. Alderson et al. (2010) investigated the mechanical properties of trichiral, tetrachiral, anti-trichiral, anti-tetrachiral and hexachiral structures. They found that anti-tetrachiral structures have high in-plane and out-of-plane elastic modulus. Gatt et al. (2013) used an analytical and numerical approach to investigate the influence of geometrical parameters on mechanical properties of anti-tetrachiral structure. They found that Poisson's ratio and elastic modulus of the anti-tetrachiral structure depend on the ratio of ligament length, thickness and bulk material properties. Chen et al. (2013) found that geometrical parameters of the anti-tetrachiral structure significantly influences the Poisson's ratio, uniaxial stiffness and transverse shear modulus. Pozniak and Wojciechowski (2014) investigated the influence of node radius, rib thickness and disorder factor on Poisson's ratio and elastic modulus of anti-tetrachiral structure. They found that thin ribs can be efficiently used as strain amplifiers due to anisotropy of the anti-tetrachiral structure. Gatt et al. (2015) investigated the effect of mode of connection between node and ligaments using an analytical and numerical approach. They observed that length to radius ratio significantly influences the stiffness of the connection between node and ligament of the structure. Mousanezhad et al. (2016) reported the influence of both hierarchy and chirality on the in-plane compression and shear properties of the cellular structure. They found that the chirality decreases Young's modulus and Poisson's ratio of the structure. Idczak and Strek (2017) used a numerical approach with method of moving asymptotes (MMA) and Solid Isotropic Material with Penalisation (SIMP) in order to increase the auxeticity of two phased materials. Using topological optimisation, they found that the proportion of hard reinforced material in a soft matrix material significantly influences the Poisson's ratio of the overall structure. Xia et al. (2018) reported that three-dimensional anti-tetrachiral structures can be used for designing the engineering structures for vibration attenuation and impact damages. They found that mechanical properties of the structure can be controlled using geometrical parameters of the unit cell. Alomarah et al. (2020a) compared the in-plane and out-of-plane compressive properties of re-entrant, hexagonal and re-entrant chiral auxetic structure (RCA). They observed that out-of-plane energy absorption of RCA structure is better than the other two structures. Tabacu et al. (2021) found that the width of the plateau region depends upon the strength of the connection between the ligament and the node. Further, they developed an analytical model to calculate the plateau stress using Bernoulli's beam model. Kai et al. (2022) studied the mechanical properties of anti-tetrachiral structure with rolled ligaments under impact loading. They found that geometrical parameters and impact velocity significantly affects the plateau strength of the structure.

From the literature review, it is evident that the majority of researchers have focused on investigating the influence of design parameters of the structures on Poisson's ratio and elastic modulus using analytical and numerical approaches. Gibson and Ashby (1997) have proved that the relative density significantly influences the mechanical properties of the auxetic structures. Still, various researchers have concentrated their efforts on investigating the properties of the well-known auxetic structures namely, re-entrant, double arrowhead, tetrachiral and hexachiral, without keeping the relative density constant. Moreover, limited literature is available related to experimental investigation on the influence of design parameters on mechanical properties of the anti-tetrachiral structure under in-plane and out-of-plane compression loading. Thus, in the present study, mechanical properties of ME fabricated anti-tetrachiral structures having in-plane and out-of-plane orientations are investigated numerically and experimentally. Further, the compressive properties and deformation mechanism of the in-plane and out-of-plane oriented structure is compared at fixed relative density for the first time. Based on mechanical characterisation of the in-plane and out-of-plane oriented specimens, the adaptability of the anti-tetrachiral structure for specific application is discussed. The influence of two design parameters, namely node radius and ligament thickness, are studied on the responses, including strength, modulus and specific energy absorption (SEA). Further, the regression models are developed, and optimisation of design parameters is performed using grey relational analysis (GRA).

2 Materials and methods

The present study involves the following steps:

1 selection of geometry of the specimen

2 design of experiments

3 numerical investigation

4 fabrication of specimens

5 mechanical testing

Each step is described briefly as under.

2.1 Geometry of specimen

In the present study, design parameters, namely node radius (r), ligament thickness (t) and ligament length (L), are considered. Figure 2 depicts a unit cell of the anti-tetrachiral structure. The relative density of structure is kept constant at 35%. The relative density is the measure of the volume fraction of the solid bulk part. As the relative density is constant, only two design parameters can be controlled, namely node radius and ligament thickness. The third parameter, i.e. ligament length, is determined using equation (1) (Lorato et al., 2010).

$$\frac{\rho}{\rho_s} = \frac{\beta[2\alpha + \pi(2-\beta)] - 2[\phi - (1-\beta)\sin\phi]}{\alpha^2} \tag{1}$$

where ρ_s = density of solid, β = t/r, α = L/r, ϕ = acos (1 – β), t = thickness of ligament, r = node radius, L = length of ligament.

Figure 2 Unit cell of anti-tetrachiral structure with design parameters

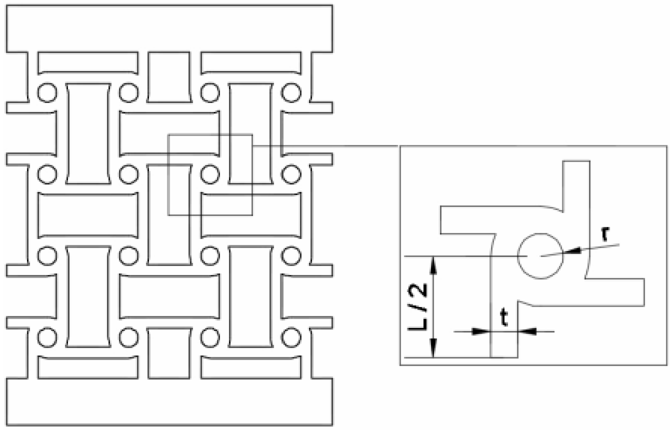

2.2 Design of experiments

Response surface method (RSM) is used to investigate the influence of several variables on response characteristics. There are two types of design of RSM namely central composite design (CCD) and Box-Behnken design (BBD). Due to absence of corners points in BBD, it can lead to inferior quality of the regression model (Myers et al., 2016). As CCD has adequate number of corner points and center points, and also it is widely used for developing second-order models, it is one of the best techniques of design of experiments in research investigation focused on studying influence of parameters on response(s). Therefore, in the present work experimental design is planned using a face-centred CCD method. Design-Expert V11 software (M/s. Stat-ease Inc.) is used to design and analyse the experiments. The range of design parameters is given in Table 1. Designed experiments include a total of 20 runs with one replication. Thus, a total of 40 experiments are planned for in-plane and out-of-plane orientations under compression loading. Tables 2 and 3 enumerate the design parameters and the corresponding configuration number for each run, respectively.

Table 1 Design parameters with corresponding range

Design parameter	*–1 level*	*0 level*	*+1 level*
Node radius (r)	1	1.625	2.25
Thickness of ligament (t)	1.2	1.6	2

2.3 Numerical investigation

Abaqus/Explicit V6.14 software is used to perform the finite element analysis (FEA) of structures. Nine sets of specimens are analysed using the FEA technique. C3D8R element is used for meshing FEA models of the structure. FEA model of the structure is shown in Figure 3(a). Initially, ACIS (Alan, Charles and Ian's system) file of the part is imported into Abaqus software. For FEA, nonlinear mechanical properties of base material are derived using compression testing of two ABS specimen of standard size

(Ø12.5 × 20 mm) as per ASTM (American Society for Testing and Materials) D695 standards. Figure 4 shows CAD model of specimen, manufactured specimen and load-displacement curves generated during compression testing. From these curves, elastic and plastic properties are calculated (Table 4) and assigned to the FEA model.

Table 2 Experimental design and specifications of the specimen for each run

Run	*Design parameters*		*Length of ligament (L) (mm)*	*Dimensions of the specimen*			
	Node radius (r) (mm)	*Thickness of ligament (t) (mm)*		*Height (mm)*	*Width (mm)*	*Depth (mm)*	*Mass (gm)*
1	2.25	1.2	10.52	52	42	25	18
2	1.625	1.2	9.60	48	38	25	15
3	2.25	1.6	13.09	62	52	25	29
4	1	1.2	8.8	45	35	25	12
5	1.625	1.2	9.60	48	38	25	15
6	1	1.6	11.18	54	44	25	21
7	1	1.6	11.18	54	44	25	21
8	1.625	2	14.5	68	58	25	35
9	1.625	1.6	12.09	58	48	25	25
10	1.625	1.6	12.09	58	48	25	25
11	2.25	1.2	10.52	52	42	25	18
12	1	2	13.5	64	54	25	31
13	2.25	2	15.3	71	61	25	39
14	2.25	2	15.3	71	61	25	39
15	1	1.2	8.8	45	35	25	15
16	2.25	1.6	13.09	62	52	25	29
17	1.625	2	14.5	68	58	25	35
18	1	2	13.5	64	54	25	31
19	1.625	1.6	12.09	58	48	25	25
20	1.625	1.6	12.09	58	48	25	25

Table 3 Configuration number and run number

Configuration no.	*Run no.*
1	1, 11
2	2, 5
3	3, 16
4	4, 15
5	6, 7
6	8, 17
7	9, 10, 19, 20
8	12, 18
9	13, 14

Table 4 Nonlinear mechanical properties of ABS material for numerical analysis

Elastic properties								
Young's modulus (MPa)	*Poisson's ratio (Ingrole et al., 2017)*					*Density (kg/m^3)*		
800	0.35					1,210		
Plastic properties								
Plastic strain	0	0.02	0.04	0.09	0.12	0.17	0.22	0.28
Plastic stress (MPa)	23.26	27.15	56.4	58.69	59.74	63.01	67.65	68.59

Figure 3 (a) FEA model of structure (b) Slicing of the STL file using Cura software (see online version for colours)

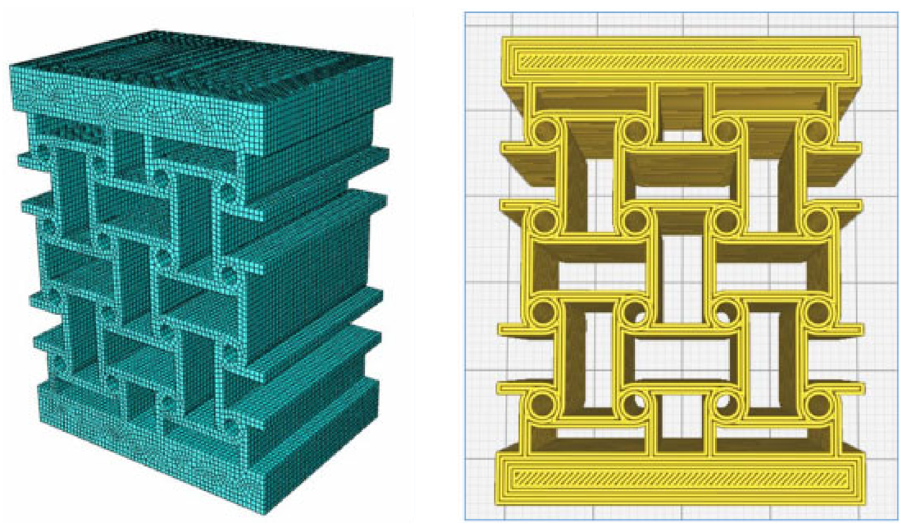

(a) (b)

Figure 4 (a) CAD model of specimen (b) Manufactured specimen (c) Load-displacement curve of specimens (see online version for colours)

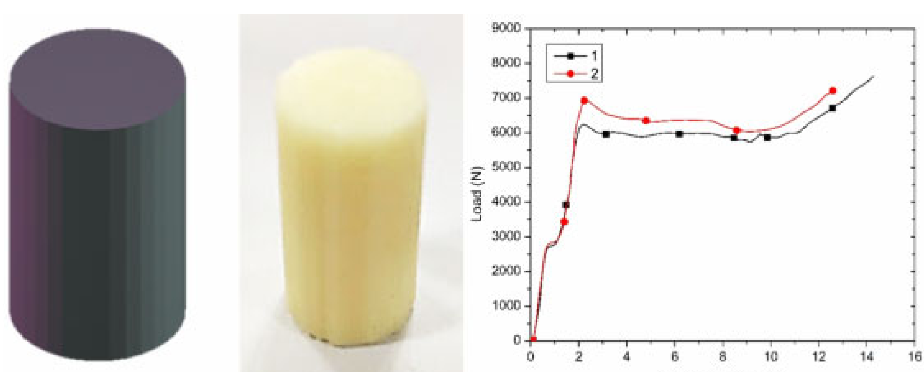

(a) (b) (c)

Mesh sensitivity analysis is performed to reduce the effect of element size on FEA results. Elements of size as 0.4, 0.6, 0.8 and 1.2 mm are considered for study. From Figure 5, it is observed that the stress-strain curve for element size of 0.6 and 0.4 mm is almost similar to the experimental results. Thus, all configurations of anti-tetrachiral structure are meshed with elements size of 0.6 mm. Multiple simulations are performed at the loading velocities of 0.05, 0.5 and 1.0 mm/s. On comparing with experimental results, it is observed that results of numerical study are less sensitive to loading velocity (Alomarah et al., 2020b). Thus, in order to reduce computational time, the loading velocity of 1.0 mm/s is used for simulation of all configurations.

Figure 5 Effect of element size of meshed model on FEA results (see online version for colours)

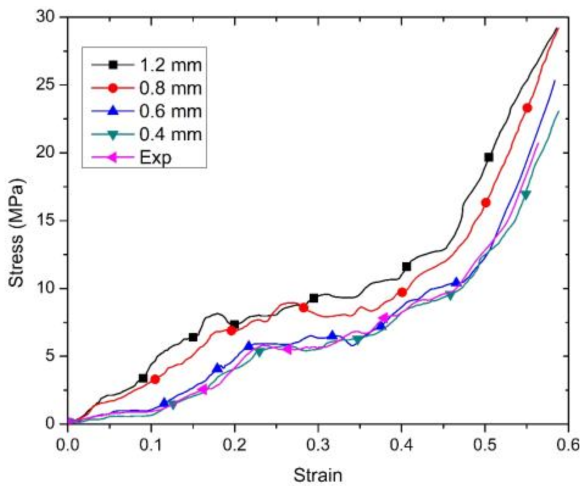

Figure 6 CAD model of anti-tetrachiral structure, (a) in-plane orientation (b) out of plane orientation (see online version for colours)

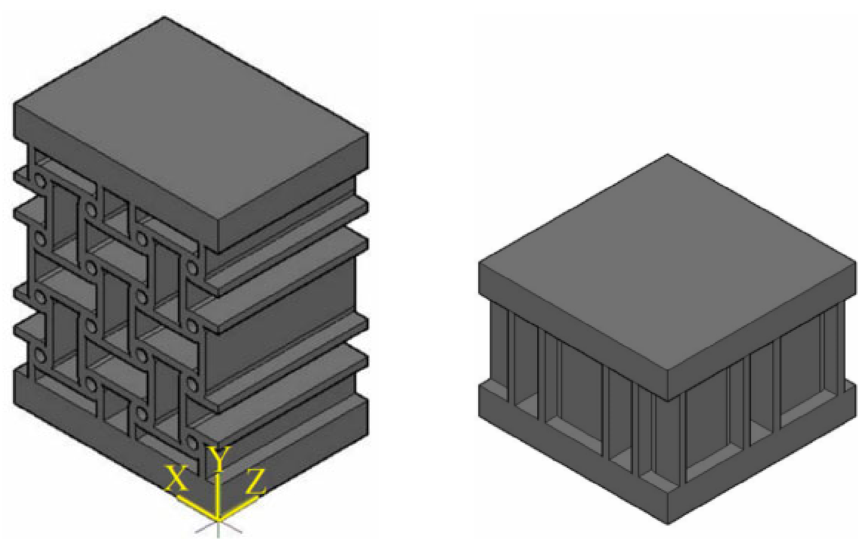

(a) (b)

In order to prevent penetration of ligaments into each other during compression loading, general contact 'All with self' is used to create the interaction. The friction coefficient for the contact surfaces is kept as 0.15. Boundary conditions are applied to the surface of the structure in order to simulate the mechanical testing. The bottom surface of the face sheet is constrained with 'encastered' in all directions, which means the surface will not move in any rotational and translational direction. The top surface is given the deformation in the negative Y-direction till 70% of strain. The rate of loading is applied in the software using values of the amplitude in boundary conditions. Results of the numerical investigation are obtained in the form of load-displacement curves. These curves are further processed using Microsoft Excel software to determine the corresponding response characteristics, namely strength, modulus and SEA.

2.4 Fabrication of specimen

According to the experimental design, the computer-aided design (CAD) model (Figure 6) of each specimen is prepared using AutoCAD 2020 software (M/s. Autodesk Inc.). The STL (Stereolithography) file of each specimen is exported from the AutoCAD 2020 software and sliced in layer-by-layer fashion using an open-source slicing software Cura V4.8.0 (M/s. Ultimaker) [Figure 3(b)]. Based on printing parameters entered to the slicing software, G-code file is generated which is fed to the printer using secure digital (SD) card. All the specimens, as shown in Figure 7 (in-plane orientation) and Figure 8 (out-of-plane orientation) are fabricated using material extrusion machine (model – Delta 2040, M/s. Wasp Inc., Italy). The build volume of the machine is Ø 200 × 400 mm^3 with printing resolution of 0.05 mm. The machine has axis accuracy of 0.012 mm in X-Y direction and 0.005 mm in Z-direction. The nozzle diameter is 0.4 mm. The samples are extruded using a filament of ABS material with 1.75 mm diameter. All the specimens are fabricated using the filament procured from the single supplier, so that variation in the material property of the filament can be minimised (Wittbrodt and Pearce, 2015). Further, the filaments are heated in oven at 800 C for six hours, so that the moisture is evaporated before printing (Halidi and Abdullah, 2012). Each specimen is printed using similar build orientation to eliminate its influence on mechanical properties of the structure (Hambali et al., 2012; Teraiya et al., 2021). Printing parameters used for the fabrication of all specimens are given in Table 5. In order to prevent the warpage of part during printing, a slurry of acetone and ABS is spread on the heated bed. Further, raft is printed at the base of each specimen to improve the adhesion of the part with the heated bed. Also, the printing speed of the raft and bottom layers of the specimen is kept at 20 mm/s, which is slower than the printing speed of the remaining specimen. Upon completion of printing, the part is carefully removed from the bed of the printer. Raft and other excessive material are separated from the part using mechanical pliers.

Dimensions of fabricated specimens are measured using a digital Vernier calliper. It is found that the dimensions of each printed specimen are similar to the dimensions of the CAD models. Further, few specimens are randomly selected, and their dimensions are checked using a coordinate measuring machine (CMM) (model – M442 Crysta Plus, make – M/s. Mituyoto Inc.) of resolution of 0.0005 mm, as shown in Figure 9. It is observed that the parts are fabricated with good dimensional accuracy. Figures 10(a) and 10(b) show enlarged image of unit cell of actual specimen and the toolpath of extruder (from Cura software), respectively. It is observed that there are presence of voids and discontinuities between the rasters of each layer.

Figure 7 Specimens for compression loading of in-plane oriented anti tetrachiral structures (see online version for colours)

Figure 8 Specimens for compression loading of out-of-plane oriented anti tetrachiral structures (see online version for colours)

Figure 9 Measurement of dimensions of the specimen using CMM (see online version for colours)

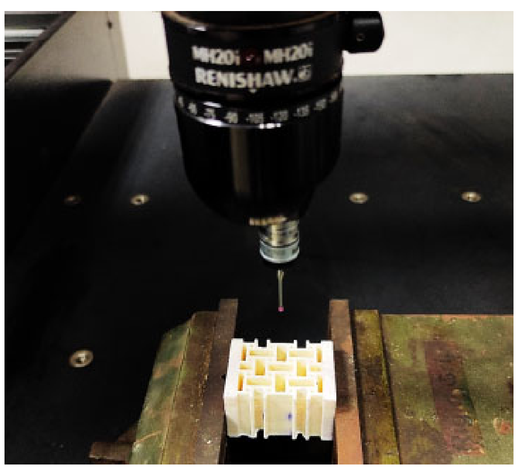

Table 5 Constant printing parameters of material extrusion

Parameter	*Value*
Build orientation	Flat (unit cell in XY plane)
Print temperature	240°C
Bed temperature	100°C
Layer height	0.2 mm
Raster angle	0°
Print speed	40 mm/s
No. of contour	01
Infill	100%

Figure 10 (a) Enlarged image of specimen (b) Toolpath of extruder (see online version for colours)

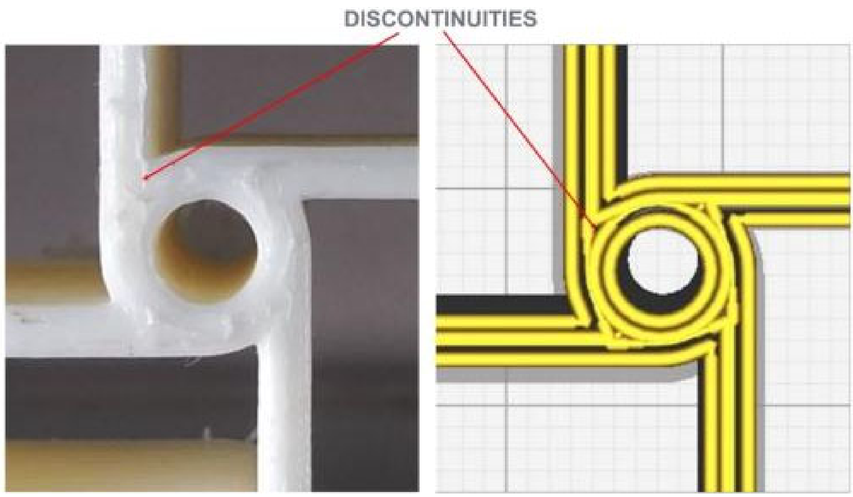

(a) (b)

2.5 Mechanical testing

Mechanical properties of fabricated specimens are measured using a universal testing machine (UTM) with a load cell of 500 kN. Figure 11 depicts the specimen and machine arrangement for conducting the compression tests for both in-plane and out-of-plane orientations. As per the experimental layout, all the specimens are tested at a constant rate of 5 mm/min. The compression load is applied till the specimen reaches the densification stage. The software of the machine provides a load-displacement curve for each tested specimen. Desired responses are calculated by post-processing of these curves. Compressive strength is a ratio of load taken by the structure up to yield point and initial cross-sectional area. Further, compression modulus is slope of stress-strain curve within the proportional limit. SEA is determined by dividing the overall area under the stress strain curve within the plateau region with density (ρ) of the structure as shown in equation (2) (Alomarah et al., 2020b).

$$\text{Specific energy absorption, } SEA = \frac{\int_0^{\varepsilon} \sigma(\varepsilon) d\varepsilon}{\rho} \tag{2}$$

Figure 11 Specimen under (a) in-plane and (b) out-of-plane compression loading using UTM (see online version for colours)

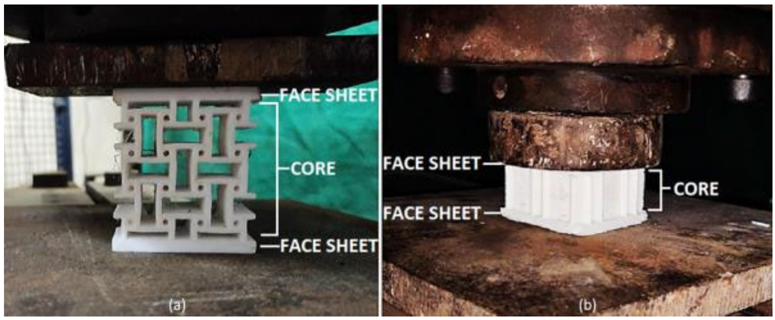

3 Results and discussion

The deformation sequence of the numerically and experimentally analysed specimen is shown in Figure 12. Stress-strain curves for FEA and experimental study for configuration number 1 with in-plane and out-of-plane orientation under compressive loading are shown in Figure 13. Due to variation in the design parameters and orientation of the structure, the response characteristics, namely compressive strength, modulus and SEA are different for each specimen. Experimental results for compression-tested anti-tetrachiral specimens with in-plane and out-of-plane orientation are given in Table 6. Based on experimental observations, the deformation mechanism and influence of design parameters for in-plane and out-of-plane orientations of the structure are discussed in the following subsections.

Figure 12 Deformation mechanism of structure under in-plane compression loading (see online version for colours)

Strain	*0*	*0.1*	*0.2*	*0.3*	*0.5*
FEA (XY-PLANE)	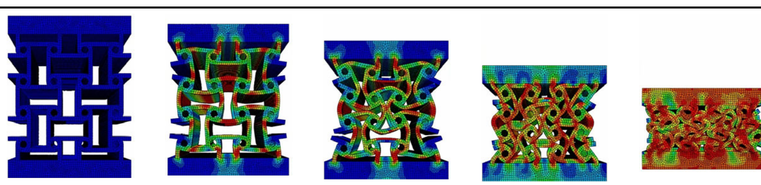				
Exp					

Figure 13 Numerical and experimental stress-strain curves for run no 1, (a) in-plane (b) out-of-plane (see online version for colours)

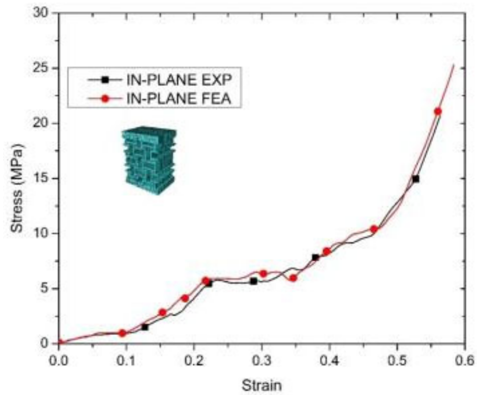

(a)

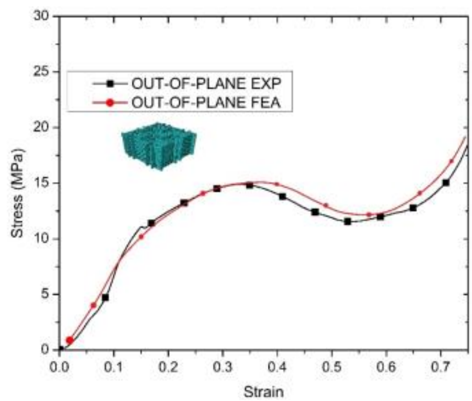

(b)

3.1 Structure under in-plane compression loading

3.1.1 Deformation mechanism

During compression testing, the vertical load is transferred to the core to face sheet of the structure, as shown in Figure 11(a). The deformation mechanism of a specimen as observed numerically and experimentally, is depicted in Figure 12. The normal load gets transferred from the vertical ligaments to the nodes. Structures undergo elastic deformation as per the mechanical properties of the bulk material. The node radius causes eccentricity in the vertical downward direction. It generates a torque around the node which develops tensile stresses on connected four ligaments. The adjacent nodes rotate in the opposite direction as they are connected on the same side of the tangential ligaments. Thus, the ligament of anti-tetrachiral structures bends in half-wave pattern as opposed to full-wave pattern of tetrachiral structures (Prall and Lakes, 1997). Each node pulls all four adjacent ligaments towards it. This creates flexural loading on the ligaments. Horizontal ligaments get wrapped around their respective nodes, which decreases the distance between adjacent nodes. This causes overall shrinkage of the specimen in the lateral direction.

Table 6 Experimental results for in-plane and out of plane compression loading of structure

Run	*Factor 1*	*Factor 2*	*In-plane orientation*			*Out of plane orientation*		
	Node radius, r (mm)	*Ligament thickness, t (mm)*	*Strength (MPa)*	*Modulus (MPa)*	*SEA (J/gm)*	*Strength (MPa)*	*Modulus (MPa)*	*SEA (J/gm)*
1	2.25	1.2	1.01	9.75	5.04	6.50	65.01	11.61
2	1.625	1.2	1.22	16.33	5.39	5.38	53.81	10.63
3	2.25	1.6	1.18	11.41	3.02	6.02	60.2	8.91
4	1	1.2	1.84	32.32	5.56	3.90	39.04	9.92
5	1.625	1.2	1.34	19.73	5.23	5.43	54.31	10.82
6	1	1.6	1.93	37.01	3.42	4.32	43.23	7.81
7	1	1.6	2.01	34.95	3.73	4.13	41.32	7.49
8	1.625	2	1.54	21.88	3.10	6.92	69.21	8.53
9	1.625	1.6	1.40	18.62	3.43	5.70	57.03	8.37
10	1.625	1.6	1.48	22.19	3.51	6.01	60.12	8.03
11	2.25	1.2	0.97	9.46	5.05	6.39	63.9	11.81
12	1	2	2.09	36.42	3.20	5.70	57.04	7.88
13	2.25	2	1.26	15.18	2.90	6.90	69.09	8.78
14	2.25	2	1.14	16.35	3.03	7.03	70.33	8.75
15	1	1.2	1.99	31.29	5.28	3.70	37.05	9.70
16	2.25	1.6	1.01	15.24	3.23	5.99	59.99	8.72
17	1.625	2	1.56	22.87	3.15	6.81	68.13	8.72
18	1	2	2.11	36.50	3.09	5.94	59.43	7.74
19	1.625	1.6	1.40	18.62	3.43	5.96	59.63	8.21
20	1.625	1.6	1.48	22.19	3.51	5.32	53.21	8.41

Figure 14 Cracks of the compression tested specimen (see online version for colours)

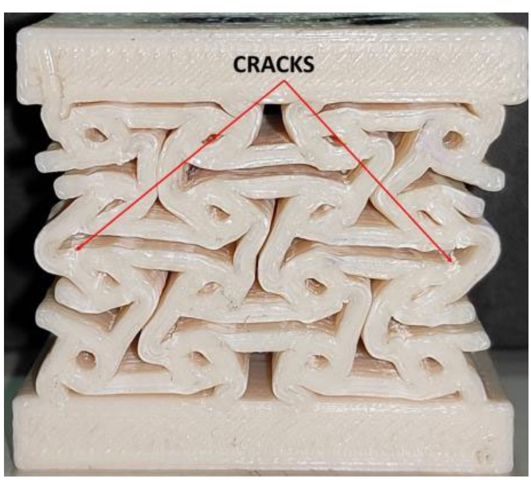

Figure 15 Stress strain curves for in-plane compression loading of all configuration of structure (see online version for colours)

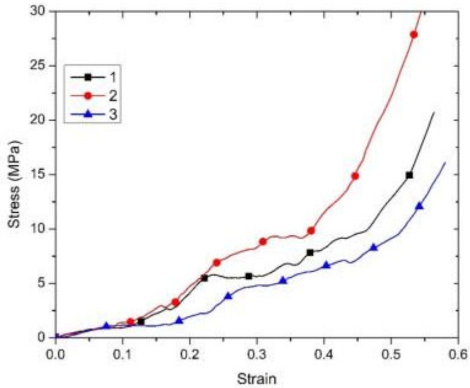

(a)

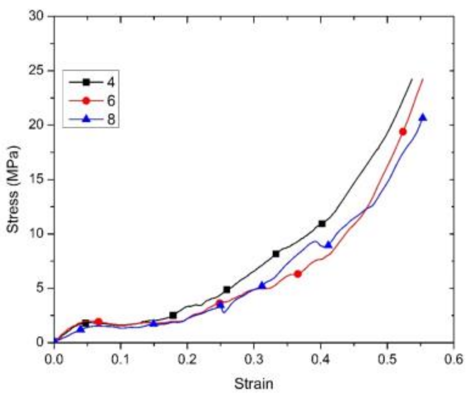

(b)

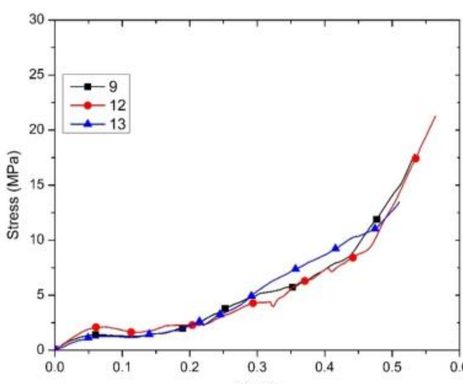

(c)

As shown in Figure 12, the middle row of nodes is least constrained among the entire specimen. So, maximum lateral deformation is observed in the middle row of the specimen. Therefore, the width of the specimen (in X-direction) is minimum at the middle of the specimen. Also, the vertical normal load is transferred to lower rows of the unit cell. Thus, flexural and buckling load are applied on the vertical ligaments, while only flexural load is applied to the horizontal ligaments. Such arrangement of nodes and ligaments causes the NPR and auxetic behaviour. With the increase in the applied load, the ligaments and nodes touch each other. At this point, the plateau region ends and densification starts. In the present structures, densification phase is observed to start at strain of 0.4. During the densification phase, the ligaments fail under the loading and get stacked. The nodes are compressed and cracks are generated at the end of the loading cycle as shown in Figure 14. Due to ductile behaviour of ABS material, the tested specimen elastically recovers some strain after the removal of load. Figure 15 shows stress-strain curves for in-plane compression loading of all configurations.

During testing of the specimens, a unique behaviour of the anti-tetrachiral structure is observed. Even during the densification phase, the structure does not cross the limit of the initial width in X-direction (Figure 12). Therefore, the structure never reaches a positive value of Poisson's ratio even during the densification phase. Other auxetic structures such as trichiral, tetrachial and hexachiral show the auxeticity up to plateau region. However, during the densification phase, they lose the structural stability and cross the dimensions in X-direction (width direction), thus lose their auxeticity (Alomarah et al., 2020a). Thus, anti-tetrachiral structures can be used in applications where the cellular structures are to be assembled such that the structure does not touch adjacent parts even after the complete failure of the structure.

3.1.2 Influence of design parameters

Table 7 lists the analysis of variance (ANOVA) for strength, modulus and SEA for compression loading of in-plane oriented structures. From ANOVA, it is observed that 'p-value' of both the design parameters is less than 0.05 for all the responses. Thus, both the design parameters significantly influence all the response characteristics.

Table 7 ANOVA results for in-plane and out-of-plane compression loading

	Parameter	*Compressive strength*		*Modulus*		*SEA*	
		F value	*p value*	*F value*	*p value*	*F value*	*p value*
In-plane	A-r	591.00	<0.05	615.12	<0.05	28.90	<0.05
	B-t	35.97	<0.05	32.89	<0.05	1,219.69	<0.05
Out of plane	A-r	290.60	<0.05	292.55	<0.05	184.36	<0.05
	B-t	150.53	<0.05	151.26	<0.05	566.20	<0.05

Figure 16(a) shows the influence of node radius and ligament thickness on compressive strength of the structure. The compressive strength increases with a decrease in node radius. With an increase in node radius, the amount of moment force also increases. This increases the flexural stresses in the ligaments. Thus, at higher values of node radius, the compressive strength reduces. Also, with an increase in thickness of ligament, the compressive strength increases. As the thickness of the ligament increases, the effective area under the compressive load increases. Therefore, the compressive strength of the part increases. Also, at higher values of ligament thickness, the area of tangential connection between the node and ligament will be higher. Thus, a higher load is required to rotate the nodes. This improves compressive strength of the structure (Gatt et al., 2015). Similar results are reported in the literature (Mousanezhad et al., 2016) for theoretical and numerical modelling of anti-tetrachiral structure under compressive loading. Based on experimental results, a regression model is developed to predict the compressive strength of anti-tetrachiral structures (Table 8). From Figure 17, it is observed that model predictions are in good agreement with experimental results.

Figure 16 Influence of design parameters during in-plane compression loading on (a) strength, (b) modulus and (c) SEA (see online version for colours)

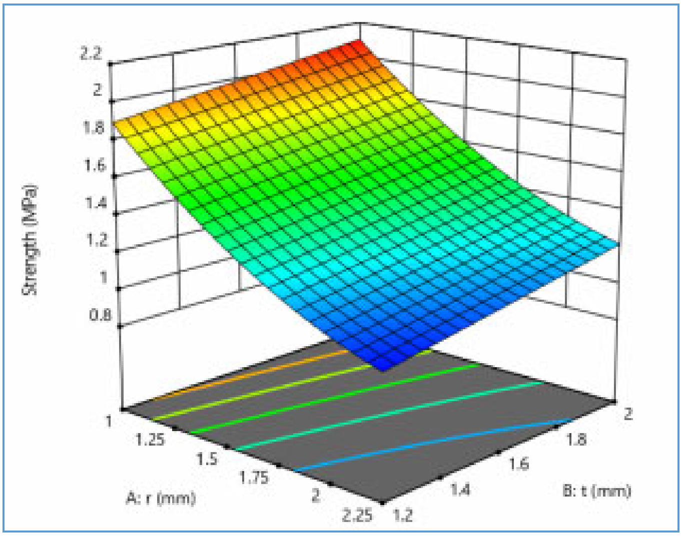

(a)

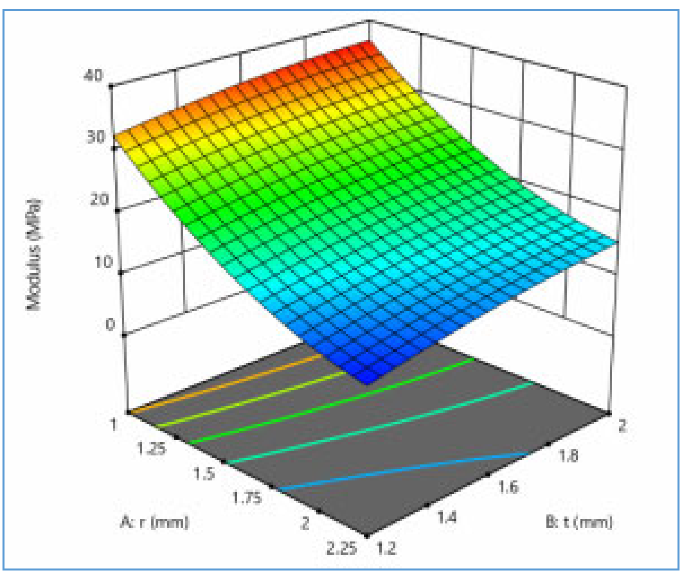

(b)

Figure 16 Influence of design parameters during in-plane compression loading on (a) strength, (b) modulus and (c) SEA (continued) (see online version for colours)

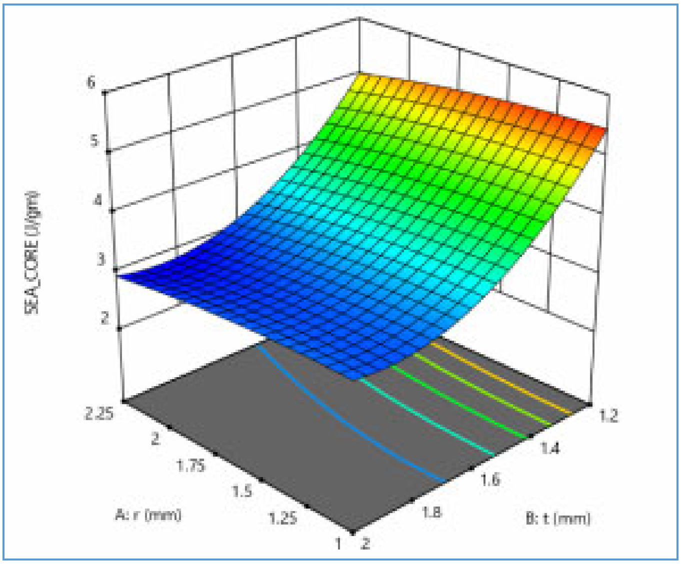

(c)

Figure 17 Actual vs. predicted graph for compressive strength under in-plane loading (see online version for colours)

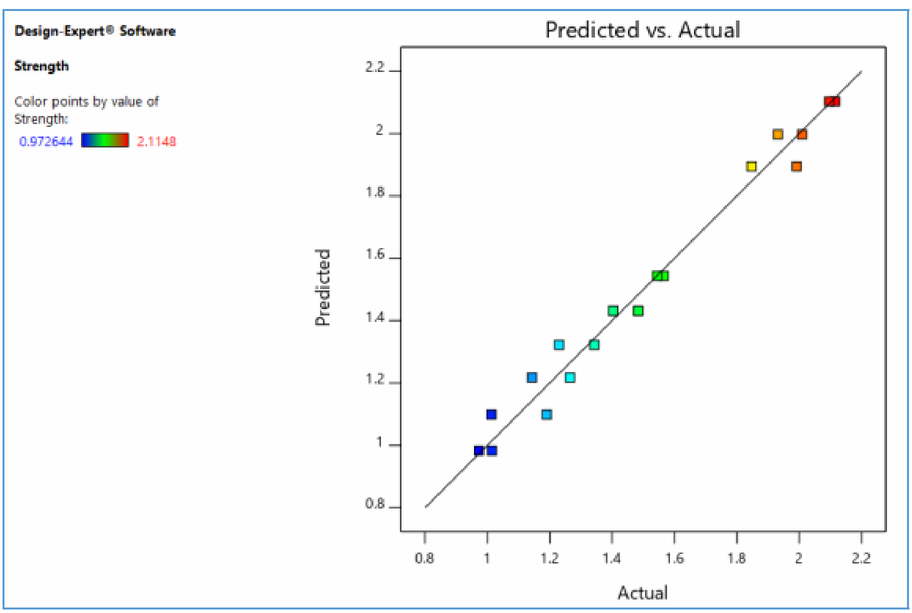

Table 8 Predictive models for compression strength, modulus and SEA

	In-plane orientation	*Out-of-plane orientation*
Compression strength	$3.038 - 1.729 \times r + 0.201 \times t + 0.025 \times r \times t + 0.298 \times r^2 + 0.011 \times t^2$	$1.972 + 7.917 \times r - 6.587 \times t - 1.493 \times r \times t - 1.244 \times r^2 + 3.338 \times t^2$
Modulus	$54.834 - 50.288 \times r + 19.853 \times t + 1.511 \times r \times t + 9.351 \times r^2 - 4.998 \times t^2$	$19.579 + 79.105 \times r - 65.634 \times t - 14.935 \times r \times t - 12.417 \times r^2 + 33.310 \times t^2$
SEA	$20.542 + 0.192 \times r - 18.542 \times t + 0.199 \times r \times t - 0.240 \times r^2 + 4.839 \times t^2$	$29.667 + 3.386 \times r - 28.309 \times t - 0.951 \times r \times t - 0.244 \times r^2 + 8.413 \times t^2$

Figure 16(b) shows the influence of node radius and ligament thickness on compressive modulus of the structure. The modulus increases with a decrease in node radius and an increase in ligament thickness. As the node radius increases, the eccentricity in the direction of loading increases. It results in an increase in moment forces, which reduces the capability of the structure to resist the deformation under compressive loading resulting in a decrease in the modulus. As ligament thickness increases, the ability of a structure to resist the deformation increases. This increases the modulus of the structure. Similar observations are reported in the literature (Alderson et al., 2010) for anti-tetrachiral structure of nylon material fabricated by selective laser sintering. They presented an analytical model for predicting the modulus as given in equation (3). It is clear from the equation that the modulus is proportional to the cube of ligament thickness and inversely proportional to node radius. The regression model for predicting the compressive modulus is given in Table 8.

$$E = \frac{E_s t^3}{6l\left(r - \frac{t}{2}\right)^2} \tag{3}$$

where E = modulus of the structure, E_s = modulus of solid bulk material, t = ligament thickness, r = node radius, l = ligament length.

Figure 16(c) shows the influence of node radius and ligament thickness on SEA of the structure. As node radius increases, the SEA reduces. As the node radius increases, the eccentricity of the applied load increases. This increases the instability of the structure. Also, as ligament thickness increases, the SEA decreases. At higher values of ligament thickness, the structure resists the deformation due to higher modulus. This results in an increase in the peak stress and earlier start of the densification phase. Thus, the area under the plateau region in the stress-strain curve decreases. Thus, overall SEA decreases with an increase in ligament thickness. Also, at higher values of node radius and ligament thickness, the area of tangential connection between the node and ligament will be higher. This increases the reaction forces and reduces the energy absorption capability of the structure. Similar results were reported by Najafi et al. (2021) for ME fabricated anti-tetrachiral structure of ABS material. The regression models for predicting the SEA are given in Table 8.

3.2 Structure under Out-of-plane compression loading

3.2.1 Deformation mechanism

Figure 18 shows a deformation mechanism of anti-tetrachiral structure positioned for out-of-plane compression loading. As the plate of the UTM starts to move, the load is applied on the top of the face sheet of the structure. This load is then transferred to the core of the structure as shown in Figure 11(b). The structure undergoes compressive stress and deforms initially within the elastic region. The nodes of the structure form a geometry of the cylinder in z-direction of the specimen; which act as a stiffener for the structure. These cylinders carry majority of load. As the stresses in the structure exceed the yield stress of the bulk material, the structure goes through plastic deformation. On further application of loading, the structure passes through the plateau region where the permanent deformation is observed. The axial compression stress causes the lateral expansion of the ligament walls in convex shape.

Figure 18 Deformation Mechanism of out-of-plane compression loading (see online version for colours)

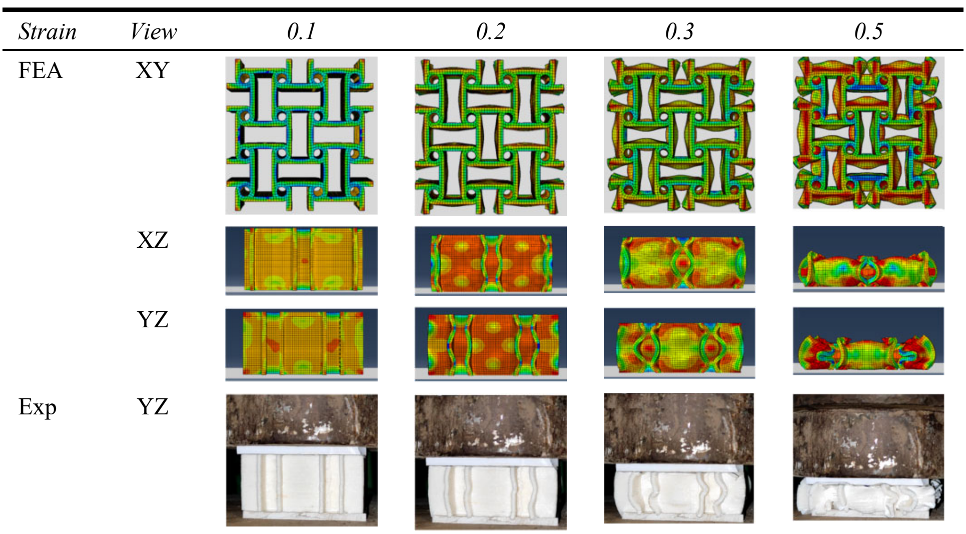

Face sheets are present on the top and bottom sides of the structure. Therefore, the deformation of unit cell in XY plane cannot be observed for out-of-plane oriented structures during experimental investigation. So, the deformation behaviour is observed using numerical simulation, as shown in Figure 19. Sides of the unit cell, namely A, F, C and H are tangent to the outer periphery of the corresponding node. Sides B, E, G and D, are tangent to the inner periphery of the node. Thus, the length of the sides AFCH is higher compared to the sides BEGD. On this longer side of the cell, the localised deformation is observed in the form of equispaced dual bulges. It creates the geometry of two hills and one valley. As the load increases, compression stresses on the structure increases resulting in increases in the size of the bulges. These bulges then get joined during the densification. On the shorter sides of the ligament wall, opposite behaviour is observed.

Figure 19 Deformation of unit cell of structure under out-of-plane compression loading (see online version for colours)

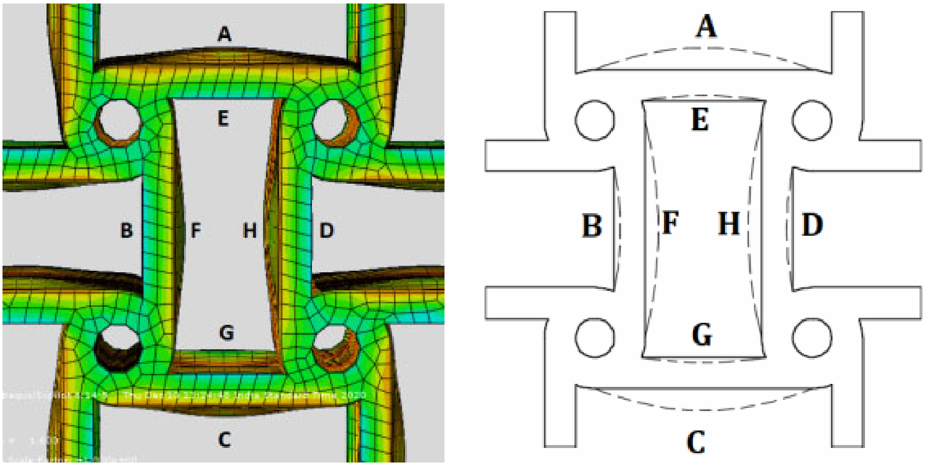

Figure 20 Stress-strain graphs for out-of-plane compression loading of all configurations (see online version for colours)

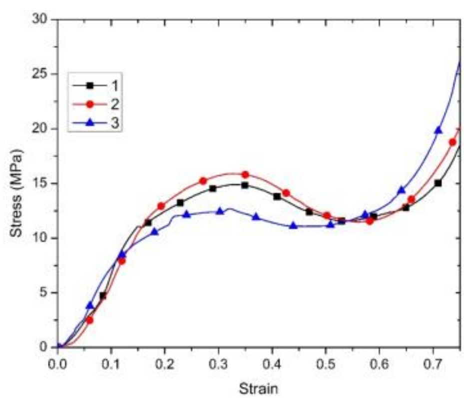

(a)

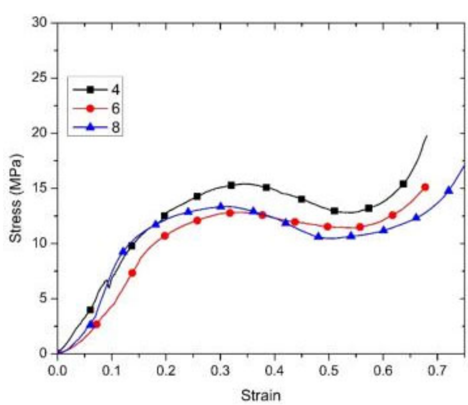

(b)

Figure 20 Stress-strain graphs for out-of-plane compression loading of all configurations (continued) (see online version for colours)

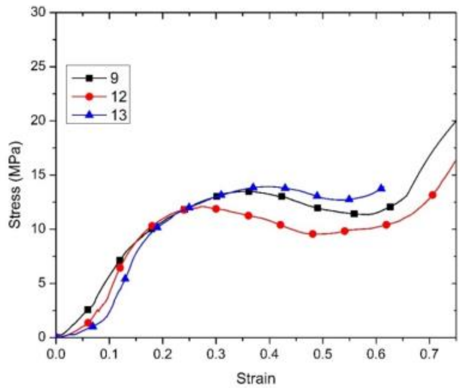

(c)

The deformation pattern of unit cells in the central region of the specimen is different from that of the cells at the edges (Xu et al., 2014). Central unit cells are highly constrained by adjacent cells compared to the unit cells at the outer edges. So, unit cells at the outer edges of the specimen undergo maximum deformation, as they do not have the support of constraining adjacent unit cells. Figure 20 shows the stress-strain curves for all configurations for compression loading of out-of-plane oriented anti-tetrachiral structures.

3.2.2 Influence of design parameters

Table 7 lists ANOVA table for compressive strength, modulus and SEA for compression loading of out-of-plane oriented structures. From the ANOVA, it is clear that all the design parameters significantly influence all the responses.

Figure 21(a) illustrates the influence of design parameters on the strength of the out-of-plane oriented anti-tetrachiral structure. With an increase in node radius and ligament thickness, the strength of the structure increases. Larger values of node radius and ligament thickness produce stronger cylinders in the Z-direction. These cylinders increase the strength of the overall structure. Therefore, the structures are able to sustain higher axial loads without plastic deformation. The regression model for predicting the values of strength is given in Table 8. From Figure 22, it is clear that model predictions are in good agreement with experimental results.

With an increase in the node radius and ligament thickness, the modulus of the structure increases. The axial arrangement of cylinders in the direction of loading resists the deformation under compressive loading. Similar observations are reported in the literature (Lorato et al., 2010) for compression testing of out-of-plane oriented anti-tetrachiral structure fabricated by selective laser sintering. The regression model for predicting the modulus is given in Table 8. Figure 21(b) illustrates the influence of design parameters on the modulus of the structure.

Figure 21 Influence of design parameters under out-of-plane compression loading for (a) strength, (b) modulus and (c) SEA (see online version for colours)

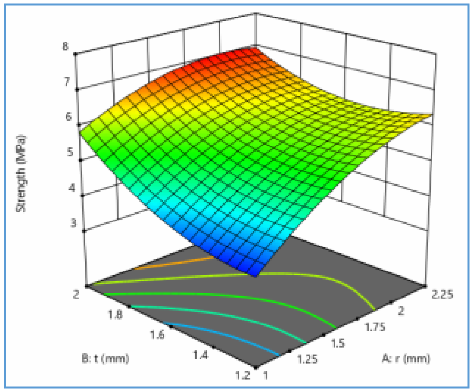

(a)

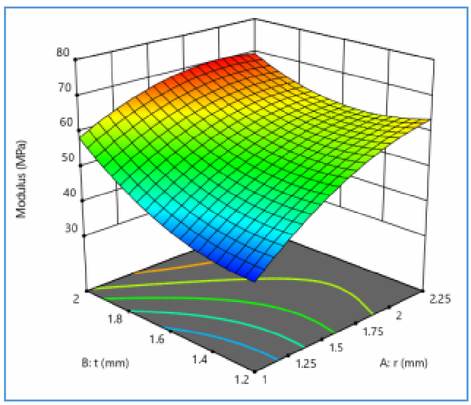

(b)

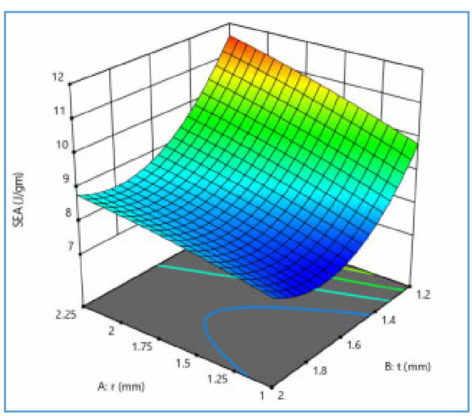

(c)

Figure 22 Actual vs. predicted graph for compressive strength under out-of-plane loading (see online version for colours)

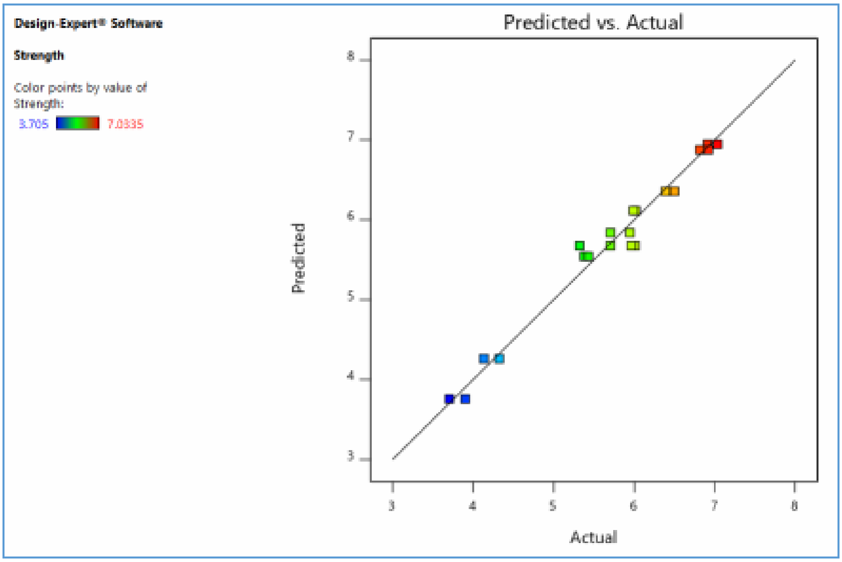

SEA increases with an increase in node radius and a decrease in ligament thickness. At a higher node radius, the structure has large cylinders. These cylinders resist deformation under the load and maintain their shape for larger stresses. Due to higher thickness, the cylinders experience higher stresses even during the plastic deformation. At higher stresses, the strain is limited; therefore, the structures go to densification phase earlier, and plateau region is narrower. So, SEA decreases at higher values of ligament thickness. Figure 21(c) illustrates the influence of design parameters on SEA of the anti-tetrachiral structure. The regression model for predicting the SEA is given in the Table 8.

3.3 Comparison of mechanical properties of in-plane and out-of-plane oriented structures

From the deformation behaviour and results of the study, comparison between mechanical properties of in-plane and out-of-plane orientation of the structure is as under:

1 It is found that the structure in out-of-plane orientation has higher strength, modulus and SEA as compared to in-plane orientation under compression loading. However, the stresses within the deformation zone or plateau zone are very high compared to the in-plane direction. These stresses transfer higher reaction forces without absorbing enough energy.

2 During compression in the in-plane direction, the structure does not have any deformation in Z-direction due to plain strain condition. It has a negative Poisson's ratio in XY-plane and zero Poisson's ratio in XZ and YZ-plane.

3 In case of out-of-plane orientation, the structure gets deformed in all directions. It has negative Poisson's ratio in the XY-plane and positive Poisson's ratio in XZ and YZ plane. So, the structure provides resistance to deformation from all directions. That is the reason for the higher strength and modulus for out-of-plane orientation as compared to in-plane orientation.

Due to the above, the unit cell of the structure should be oriented in the in-plane direction when the application necessitates higher energy absorption at minimum peak stress. One of such applications is, improving the crashworthiness of passenger vehicles. The crumple zone of the car is designed in such a way that it absorbs the majority of impact energy and provides enough occupant safety. While the unit cell of structure should be oriented in an out-of-plane direction when the application demands higher strength and modulus. For example, in case of wind turbine blades and aircraft propellers, out-of-plane orientated anti-tetrachiral structures are most suitable (Wu et al., 2019).

3.4 Comparison of Results of Experimental and Numerical Investigation

The deformation sequence of the compression tested specimen is found similar for both the experimental and numerical investigation. The value of various response characteristics and percentage deviation between experimental and numerical results are listed in the Table 9. The percentage difference between experimental and numerical results is less than 15%. Thus, experimental results are in good agreement with numerical results.

Table 9 Comparison of FEA and experimental results

			Strength (MPa)			*Modulus (MPa)*			*SEA (J/gm)*		
	r (mm)	*t (mm)*	*Experimental*	*FEA*	*(%) Deviation*	*Experimental*	*FEA*	*(%) Deviation*	*Experimental*	*FEA*	*(%) Deviation*
In-plane	1.625	1.6	1.40	1.49	6.50	18.62	20.04	7.63	3.43	3.75	9.23
	2.25	1.2	0.97	1.08	11.71	9.46	10.33	9.22	5.05	5.53	9.46
	1.625	2	1.54	1.38	10.63	21.88	19.96	8.79	3.10	3.45	11.43
Out of plane	1	1.6	4.32	4.87	12.71	43.23	42.87	12.71	7.81	8.82	12.92
	1.625	1.2	5.38	5.72	6.32	53.81	57.20	6.32	10.63	9.42	11.41
	2.25	1.2	6.39	6.94	8.53	63.90	69.40	8.53	11.81	10.72	9.19

3.5 Confirmation tests

For confirmation tests, the experiments are performed at random levels of design parameters. Table 10 gives the results of the confirmation test. It is observed that the deviation of observed values from predicted values is less than 12%. Thus, the results of the confirmation tests are in good agreement with predictive models.

Table 10 Confirmation test at random level of design parameters

			Strength (MPa)			*Modulus (MPa)*			*SEA (J/gm)*		
	r (mm)	*t (mm)*	*Experimental*	*FEA*	*(%) Deviation*	*Experimental*	*FEA*	*(%) Deviation*	*Experimental*	*FEA*	*(%) Deviation*
In-plane	1.625	1.2	1.32	1.48	12.31	17.38	15.33	11.79	5.33	4.88	8.47
	1	1.6	2.00	1.81	9.25	35.28	32.61	7.58	3.53	3.13	11.31
	2.25	1.6	1.10	0.97	11.31	13.44	14.48	7.75	3.20	2.91	8.84
Out of plane	1	1.6	4.29	4.74	10.56	42.16	46.61	10.56	7.56	6.91	8.56
	2.25	1.2	5.42	4.90	9.59	54.01	59.18	9.59	10.83	11.87	9.68
	2.25	2	7.09	7.82	10.37	70.1	62.83	10.37	8.81	9.80	11.33

3.6 Optimisation using grey relational analysis

Optimisation of design parameters of anti-tetrachiral auxetic structure is performed to maximise the strength, modulus and SEA using grey relational analysis (GRA). GRA is one of the most widely used multiple attribute decision making (MADM) technique. It is employed to find best alternative among the available design parameter combination with a goal of achieving optimised response characteristics which may be conflicting with each other. GRA is most useful technique while dealing with poor, incomplete, and uncertain information (Lin et al., 2006). Based on results available from the experiments, various steps of GRA are performed, namely, normalisation of response, deviation sequence, grey relational grade and ranking. The structure which has the best ranking is designated as the optimum configuration. Table 11 and 12 lists the GRA of the in-plane and out-of-plane oriented anti-tetrachiral structures under compression loading, respectively. Grey relational grade (GRG) of the following configuration is observed to be highest:

1 for in-plane orientation – the configuration 4 (run 4, 15) having design parameters, node radius 1 mm and ligament thickness 1.2 mm

2 For out-of-plane orientation – the configuration 1 (run 1, 11) having design parameters, node radius 1.625 mm and ligament thickness 1.2 mm.

Table 11 GRA of the in-plane compression loading of anti-tetrachiral structures

Run	*Experimental results*			*Normalised values*			*Deviation sequence*			*Grey relational coefficient*			*Grade*	*Rank*
	Strength	*Modulus*	*SEA*	*Strength*	*Modulus*	*SEA*	*Strength*	*Modulus*	*SEA*	*Strength*	*Modulus*	*SEA*		
1	1.01	9.75	5.04	0.04	0.01	0.80	0.96	0.99	0.20	0.38	0.38	0.75	0.50	9
2	1.23	16.33	5.40	0.23	0.25	0.94	0.77	0.75	0.06	0.44	0.44	0.90	0.59	8
3	1.19	11.42	3.02	0.19	0.07	0.05	0.81	0.93	0.95	0.43	0.39	0.39	0.40	20
4	1.85	32.33	5.57	0.77	0.83	1.00	0.23	0.17	0.00	0.72	0.78	1.00	0.83	1
5	1.34	19.73	5.24	0.32	0.37	0.88	0.68	0.63	0.12	0.47	0.49	0.83	0.60	7
6	1.93	37.01	3.42	0.84	1.00	0.20	0.16	0.00	0.80	0.79	1.00	0.43	0.74	6
7	2.01	34.96	3.73	0.91	0.93	0.31	0.09	0.07	0.69	0.87	0.89	0.47	0.74	5
8	1.54	21.88	3.10	0.50	0.45	0.07	0.50	0.55	0.93	0.55	0.52	0.39	0.49	14
9	1.40	18.63	3.43	0.38	0.33	0.20	0.62	0.67	0.80	0.49	0.47	0.43	0.46	15
10	1.48	22.19	3.51	0.45	0.46	0.23	0.55	0.54	0.77	0.52	0.53	0.44	0.50	12
11	0.97	9.47	5.06	0.00	0.00	0.81	1.00	1.00	0.19	0.38	0.38	0.76	0.50	10
12	2.10	36.42	3.20	0.98	0.98	0.11	0.02	0.02	0.89	0.97	0.97	0.40	0.78	4
13	1.26	15.19	2.90	0.26	0.21	0.00	0.74	0.79	1.00	0.45	0.43	0.38	0.42	17
14	1.14	16.35	3.03	0.15	0.25	0.05	0.85	0.75	0.95	0.41	0.44	0.39	0.41	18
15	1.99	31.30	5.29	0.89	0.79	0.90	0.11	0.21	0.10	0.85	0.74	0.85	0.81	2
16	1.01	15.24	3.23	0.03	0.21	0.12	0.97	0.79	0.88	0.38	0.43	0.41	0.41	19
17	1.57	22.87	3.15	0.52	0.49	0.09	0.48	0.51	0.91	0.56	0.54	0.40	0.50	11
18	2.11	36.50	3.09	1.00	0.98	0.07	0.00	0.02	0.93	1.00	0.97	0.39	0.79	3
19	1.40	18.63	3.43	0.38	0.33	0.20	0.62	0.67	0.80	0.49	0.47	0.43	0.46	15
20	1.48	22.19	3.51	0.45	0.46	0.23	0.55	0.54	0.77	0.52	0.53	0.44	0.50	12

Table 12 GRA of the out-of-plane compression loading of anti-tetrachiral structures

Run	*Experimental results*			*Normalised values*			*Deviation sequence*			*Grey relational coefficient*			*Grade*	*Rank*
	Strength	*Modulus*	*SEA*	*Strength*	*Modulus*	*SEA*	*Strength*	*Modulus*	*SEA*	*Strength*	*Modulus*	*SEA*		
1	6.50	65.01	11.61	0.84	0.84	0.95	0.16	0.16	0.05	0.79	0.79	0.93	0.84	2
2	5.38	53.81	10.63	0.50	0.50	0.73	0.50	0.50	0.27	0.55	0.55	0.69	0.59	9
3	6.02	60.20	8.91	0.70	0.70	0.33	0.30	0.30	0.67	0.66	0.66	0.47	0.60	8
4	3.90	39.04	9.92	0.06	0.06	0.56	0.94	0.94	0.44	0.39	0.39	0.58	0.45	17
5	5.43	54.31	10.82	0.52	0.52	0.77	0.48	0.48	0.23	0.55	0.55	0.72	0.61	7
6	4.32	43.23	7.81	0.19	0.19	0.07	0.81	0.81	0.93	0.42	0.42	0.39	0.41	19
7	4.13	41.32	7.50	0.13	0.13	0.00	0.87	0.87	1.00	0.41	0.41	0.38	0.40	20
8	6.92	69.21	8.54	0.97	0.97	0.24	0.03	0.03	0.76	0.95	0.95	0.44	0.78	5
9	5.70	57.03	8.38	0.60	0.60	0.20	0.40	0.40	0.80	0.60	0.60	0.43	0.54	14
10	6.01	60.12	8.03	0.69	0.69	0.12	0.31	0.31	0.88	0.66	0.66	0.41	0.58	11
11	6.39	63.90	11.82	0.81	0.81	1.00	0.19	0.19	0.00	0.76	0.76	1.00	0.84	1
12	5.70	57.04	7.89	0.60	0.60	0.09	0.40	0.40	0.91	0.60	0.60	0.40	0.53	15
13	6.91	69.09	8.79	0.96	0.96	0.30	0.04	0.04	0.70	0.94	0.94	0.46	0.78	4
14	7.03	70.33	8.75	1.00	1.00	0.29	0.00	0.00	0.71	1.00	1.00	0.46	0.82	3
15	3.71	37.05	9.70	0.00	0.00	0.51	1.00	1.00	0.49	0.38	0.38	0.55	0.43	18
16	5.99	59.99	8.72	0.69	0.69	0.28	0.31	0.31	0.72	0.66	0.66	0.46	0.59	10
17	6.81	68.13	8.72	0.93	0.93	0.28	0.07	0.07	0.72	0.90	0.90	0.46	0.75	6
18	5.94	59.43	7.75	0.67	0.67	0.06	0.33	0.33	0.94	0.65	0.65	0.39	0.56	13
19	5.96	59.63	8.21	0.68	0.68	0.17	0.32	0.32	0.83	0.65	0.65	0.42	0.57	12
20	5.32	53.21	8.42	0.49	0.49	0.21	0.51	0.51	0.79	0.54	0.54	0.43	0.50	16

4 Conclusions

The present article is focused on numerical and experimental investigation of design parameters on mechanical properties of ME fabricated anti-tetrachiral structures under in-plane and out-of-plane compressive loading. Major findings of the study are as follows -

1. both the design parameters, namely node radius and ligament thickness, significantly influence all the responses such as strength, modulus, and SEA in both the in-plane and out-of-plane compressive loading
2. for in-plane orientation of structure, strength and modulus increase with decrease in node radius and increase in ligament thickness while SEA increases with decrease in node radius and ligament thickness
3. for out-of-plane orientation of structure, strength and modulus increase with increase in node radius and ligament thickness while SEA increases with increase in node radius and decrease in ligament thickness
4. stresses in the plateau region are minimum and remain almost constant till the densification phase during in-plane orientation of the structure, which is ideal for energy absorbing applications
5. strength and modulus of the structure are higher in out-of-plane structure, therefore this type of orientation is desirable in applications where high strength is needed.

Results of numerical and experimental investigation are found to be in good agreement. Based on experimental results, the regression models are developed to predict the strength, modulus, and SEA. The parameters are optimised using GRA technique to maximise the responses. Results of the confirmation tests show good agreement with the proposed regression model. In-plane oriented anti-tetrachiral structures are suitable for packaging and front car bumper, while out-of-plane oriented structures are suitable for aircraft propellers and wind turbine blades.

References

Abramovitch, H., Burgard, M., Edery-Azulay, L., Evans, K.E., Hoffmeister, M., Miller, W., Scarpa, F., Smith, C.W. and Tee, K.F. (2010) 'Smart tetrachiral and hexachiral honeycomb: sensing and impact detection', *Composites Science and Technology*, Vol. 70, No. 7, pp.1072–1079.

Alderson, A., Alderson, K.L., Attard, D., Evans, K.E., Gatt, R., Grima, J.N., Miller, W., Ravirala, N., Smith, C.W. and Zied, K. (2010) 'Elastic constants of 3-, 4- and 6-connected chiral and anti-chiral honeycombs subject to uniaxial in-plane loading', *Composites Science and Technology*, Vol. 70, No. 7, pp.1042–1048.

Alderson, A., Rasburn, J., Ameer-Beg, S., Mullarkey, P.G., Perrie, W. and Evans, K.E. (2000) 'An auxetic filter: a tuneable filter displaying enhanced size selectivity or defouling properties', *Industrial & Engineering Chemistry Research*, Vol. 39, No. 3, pp.654–665.

Alomarah, A., Masood, S.H. and Ruan, D. (2020a) 'Out-of-plane and in-plane compression of additively manufactured auxetic structures', *Aerospace Science and Technology*, Vol. 106, p.106107.

Alomarah, A., Masood, S.H., Sbarski, I., Faisal, B., Gao, Z. and Ruan, D. (2020b) 'Compressive properties of 3D printed auxetic structures: experimental and numerical studies', *Virtual and Physical Prototyping*, Vol. 15, No. 1, pp.1–21.

Ashby, M.F. (2006) 'The properties of foams and lattices', *Philosophical Transactions of the Royal Society A: Mathematical, Physical and Engineering Sciences*, Vol. 364, No. 1838, pp.15–30.

Bezazi, A. and Scarpa, F. (2007) 'Mechanical behaviour of conventional and negative Poisson's ratio thermoplastic polyurethane foams under compressive cyclic loading', *International Journal of Fatigue*, Vol. 29, No. 5, pp.922–930.

Boparai, K.S. and Singh, R. (2019) '3D printed functional prototypes for electrochemical energy storage', *International Journal of Materials Engineering Innovation*, Vol. 10, No. 2, pp.152–164.

Chen, Y.J., Scarpa, F., Liu, Y.J. and Leng, J.S. (2013) ''Elasticity of anti-tetrachiral anisotropic lattices', *International Journal of Solids and Structures*, Vol. 50, No. 6, pp.996–1004.

Dalela, S., Balaji, P.S. and Jena, D.P. (2021) 'A review on application of mechanical metamaterials for vibration control', *Mechanics of Advanced Materials and Structures*, pp.1–26, https://doi.org/10.1080/15376494.2021.1892244.

Fernandes, M.G., Alves, J.L. and Fonseca, E.M.M. (2016) 'Diaphyseal femoral fracture: 3D biomodel and intramedullary nail created by additive manufacturing', *International Journal of Materials Engineering Innovation*, Vol. 7, No. 2, pp.130–142.

Gatt, R., Attard, D., Farrugia, P.S., Azzopardi, K.M., Mizzi, L., Brincat, J.P. and Grima, J.N. (2013) 'A realistic generic model for anti-tetrachiral systems: A realistic generic model for anti-tetrachiral systems'. *Physica Status Solidi B*, Vol. 250, No. 10, pp.2012–2019.

Gatt, R., Brincat, J.P., Azzopardi, K.M., Mizzi, L. and Grima, J.N. (2015) 'On the effect of the mode of connection between the node and the ligaments in anti-tetrachiral systems: connections between nodes and ligaments in anti-tetrachirals' *Advanced Engineering Materials*, Vol. 17, No. 2, pp.189–198.

Gibson, I., Rosen, D. and Stucker, B. (2015) *Additive Manufacturing Technologies: 3D Printing, Rapid Prototyping, and Direct Digital Manufacturing*, 2nd ed., Springer, New York, NY.

Gibson, L. and Ashby, M.F. (1997) *Cellular Solids: Structure and Properties*, Cambridge University Press, Cambridge, UK.

Grima, J.N., Gatt, R. and Farrugia, P.S. (2008) 'On the properties of auxetic meta-tetrachiral structures', *Physica Status Solidi B*, Vol. 245, No. 3, pp.511–520.

Halidi, S.N.A.M. and Abdullah, J. (2012) 'Moisture effects on the ABS used for Fused Deposition Modeling rapid prototyping machine', *2012 IEEE Symposium on Humanities, Science and Engineering Research*, pp.839–843.

Hambali, R.H., Smith, P. and Rennie, A.E.W. (2012) 'Determination of the effect of part orientation to the strength value on additive manufacturing FDM for end-use parts by physical testing and validation via three-dimensional finite element analysis', *International Journal of Materials Engineering Innovation*, Vol. 3, Nos. 3–4, pp.269–281.

Idczak, E. and Strek, T. (2017) 'Minimization of Poisson's ratio in anti-tetra-chiral two-phase structure', *Materials Science and Engineering*, Vol. 248, No. 1, p.012006.

Imbalzano, G., Tran, P., Ngo, T.D. and Lee, P.V. (2017) 'Three-dimensional modelling of auxetic sandwich panels for localised impact resistance', *Journal of Sandwich Structures & Materials*, Vol. 19, No. 3, pp.291–316.

Ingrole, A., Hao, A. and Liang, R. (2017) 'Design and modeling of auxetic and hybrid honeycomb structures for in-plane property enhancement', *Materials & Design*, Vol. 117, pp.72–83.

Kai, L., Xiaofei, C., Peng, Z. and Ying, L. (2022) 'Dynamic mechanical performances of enhanced anti-tetra-chiral structure with rolled cross-section ligaments under impact loading', *International Journal of Impact Engineering*, Vol. 166, p.104204.

Kolken, H.M. and Zadpoor, A.A. (2017) 'Auxetic mechanical metamaterials'. *RSC Adv.*, Vol. 7, No. 9, pp.5111–5129.

Kumar, P., Ahuja, I.P.S. and Singh, R. (2012) 'Application of fusion deposition modelling for rapid investment casting – a review', *International Journal of Materials Engineering Innovation*, Vol. 3, Nos. 3–4, pp.204–227.

Kumar, S., Vyavahare, S., Teraiya, S. and Dhakar, L.C. (2021) ‘Experimental investigation on fdm fabricated tetra chiral auxetic structures under uniaxial compressive loading’, in Dave, H.K. and Davim, J.P. (Eds.): *Fused Deposition Modeling Based 3D Printing, Materials Forming, Machining and Tribology*, pp.63–83, Springer, Cham.

Kumar, S.S. and Vinodh, S. (2019) ‘Application of interpretive structural modelling for analysis of factors influencing composite fabrication using additive manufacturing’, *International Journal of Materials Engineering Innovation*, Vol. 10, No. 3, pp.218–245.

Lakes, R. (1987) ‘Foam structures with a negative Poisson’s ratio’, *Science (New York, NY)*, Vol. 235, No. 4792, pp.1038–1040.

Larcher, M. (2011) ‘Risk analysis about explosions in train carriages’, *International Journal of Materials Engineering Innovation*, Vol. 2, No. 2, pp.110-123.

Lin, C.T., Chang, C.W. and Chen, C.B. (2006) ‘The worst ill-conditioned silicon wafer slicing machine detected by using grey relational analysis’, *International Journal of Advanced Manufacturing Technology*, Vol. 31, No. 3, pp.388–395.

Lorato, A., Innocenti, P., Scarpa, F., Alderson, A., Alderson, K.L., Zied, K.M., Ravirala, N., Miller, W., Smith, C.W. and Evans, K.E. (2010) ‘The transverse elastic properties of chiral honeycombs’, *Composites Science and Technology*, Vol. 70, No. 7, pp.1057–1063.

Meneses, A.D., Alves, J.L. and Lopes, L. (2016) ‘Study of 3D printing potential in supporting the manufacturing process of shoes for people with cerebral palsy’, *International Journal of Materials Engineering Innovation*, Vol. 7, Nos. 3–4, pp.184–199.

Mousanezhad, D., Haghpanah, B., Ghosh, R., Hamouda, A.M., Nayeb-Hashemi, H. and Vaziri, A. (2016) ‘Elastic properties of chiral, anti-chiral, and hierarchical honeycombs: A simple energy-based approach’ *Theoretical and Applied Mechanics Letters*, Vol. 6, No. 2, pp.81–96.

Myers, R.H., Montgomery, D.C. and Anderson-Cook, C.M. (2016) *Response Surface Methodology: Process and Product Optimization Using Designed Experiments*, John Wiley & Sons, New York, USA.

Najafi, M., Ahmadi, H. and Liaghat, G. (2021) ‘Experimental investigation on energy absorption of auxetic structures’, *Materials Today: Proceedings*, Vol. 34, pp.350–355.

Paulino, M., Teixeira-Dias, F., Gameiro, C.P. and Cirne, J. (2009) ‘Hyperelastic and dynamical behaviour of cork and its performance in energy absorption devices and crashworthiness applications’, *International Journal of Materials Engineering Innovation*, Vol. 1, No. 2, pp.197–234.

Pozniak, A.A. and Wojciechowski, K.W. (2014) ‘Poisson’s ratio of rectangular anti-chiral structures with size dispersion of circular nodes’ *Physica Status Solidi B,* Vol. 251, No. 2, pp.367–374.

Prall, D. and Lakes, R.S. (1997) ‘Properties of a chiral honeycomb with a Poisson’s ratio of – 1’, *International Journal of Mechanical Sciences*, Vol. 39, No. 3, pp.305–314.

Sarvestani, H.Y., Akbarzadeh, A.H., Niknam, H. and Hermenean, K. (2018) ‘3D printed architected polymeric sandwich panels: energy absorption and structural performance’, *Composite Structures*, Vol. 200, pp.886–909.

Scarpa, F., Bullough, W.A. and Lumley, P. (2004) ‘Trends in acoustic properties of iron particle seeded auxetic polyurethane foam’, *Proceedings of the Institution of Mechanical Engineers, Part C: Journal of Mechanical Engineering Science*, Vol. 218, No. 2, pp.241–244.

Singh, J.P. and Pandey, P.M. (2015) ‘Experimental investigations and statistical analysis of regular open cell porous metallic structure fabricated through rapid manufacturing’, *International Journal of Materials Engineering Innovation*, Vol. 6, Nos. 2–3, pp.91–107.

Sousa-Martins, J. and Teixeira-Dias, F. (2011) ‘Using natural cellular materials to improve blast-wave protection’ *International Journal of Materials Engineering Innovation*, Vol. 2, No. 2, pp.165–178.

Tabacu, S., Predoiu, P. and Negrea, R. (2021) ‘A theoretical model for the estimate of plateau force for the crushing process of 3D auxetic anti-tetra chiral structures’, *International Journal of Mechanical Sciences*, Vol. 199, p.106405.

Teraiya, S., Vyavahare, S. and Kumar, S. (2021) 'Experimental Investigation on influence of process parameters on mechanical properties of PETG parts made by fused deposition modelling', *Advances in Manufacturing Processes*, pp.283–293, Springer, Singapore.

Vesenjak, M., Ren, Z. and Ochsner, A. (2009) 'Dynamic behaviour of regular closed-cell porous metals–computational study', *International Journal of Materials Engineering Innovation*, Vol. 1, No. 2, pp.175-196.

Vyavahare, S. and Kumar, S. (2020) 'Re-entrant auxetic structures fabricated by fused deposition modeling: an experimental study of influence of process parameters under compressive loading', *Polymer Engineering & Science*, Vol. 60, No. 12, pp.3183–3196.

Vyavahare, S. and Kumar, S. (2021) 'Numerical and experimental investigation of FDM fabricated re-entrant auxetic structures of ABS and PLA materials under compressive loading', *Rapid Prototyping Journal*, Vol. 27, No. 2, pp.223–244.

Wittbrodt, B. and Pearce, J.M. (2015) 'The effects of PLA color on material properties of 3-D printed components', *Additive Manufacturing*, Vol. 8, pp.110–116.

Wu, T., Li, M., Zhu, X. and Lu, X. (2021) 'Research on non-pneumatic tire with gradient anti-tetrachiral structures'. *Mechanics of Advanced Materials and Structures*, Vol. 28, No. 22, pp.2351–2359, https://doi.org/10.1080/15376494.2020.1734888.

Wu, W., Hu, W., Qian, G., Liao, H., Xu, X. and Berto, F. (2019) 'Mechanical design and multifunctional applications of chiral mechanical metamaterials: a review', *Materials & Design*, Vol. 180, p.107950.

Xia, R., Song, X., Sun, L., Wu, W., Li, C., Cheng, T. and Qian, G. (2018) 'Mechanical properties of 3D isotropic anti-tetrachiral metastructure', *Physica Status Solidi B*, Vol. 255, No. 4, p.1700343.

Xu, P., Zhao, H., Yao, S., Che, Q., Xing, J., Huang, Q. and Xu, K. (2020) 'Multi-objective optimisation of a honeycomb-filled composite energy absorber for subway vehicles', *International Journal of Crashworthiness*, Vol. 25, No. 6, pp.603–611.

Xu, S., Ruan, D. and Beynon, J.H. (2014) 'Finite element analysis of the dynamic behavior of aluminum honeycombs', *International journal of computational methods*, Vol. 11, No. Supp01, p.134400.

Zhu, F., Wang, Z., Lu, G. and Ruan, D. (2009) 'The impulsive response of aluminium foam core sandwich structures', *International Journal of Materials Engineering Innovation*, Vol. 1, No. 2, pp.133–153.